Exploring the Potentiality of Natural Products from Essential Oils as Inhibitors of Odorant-Binding Proteins: A Structure- and Ligand-Based Virtual Screening Approach To Find Novel Mosquito Repellents

Kauê Santana da Costa,*,[†] João Marcos Galúcio,[†] Clauber Henrique Souza da Costa,[‡] Amanda Ruslana Santana,[‡] Vitor dos Santos Carvalho,[‖] Lidiane Diniz do Nascimento,[§] Anderson Henrique Lima e Lima,[‖] Jorddy Neves Cruz,[‡] Claudio Nahum Alves,[‖] and Jerônimo Lameira*,[⊥]

[†]Institute of Biodiversity, Federal University of Western Pará, 68035-110 Santarém, Pará, Brazil
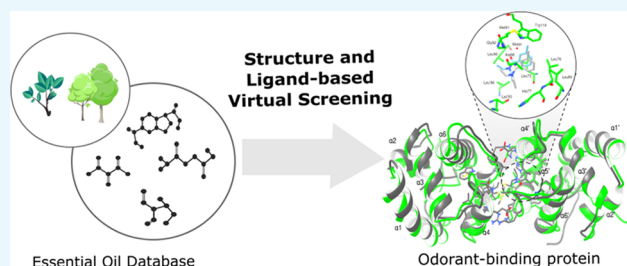
[‡]Department of Pharmaceutical Sciences, Federal University of Pará, 66060-902 Belém, Pará, Brazil

[§]Museu Paraense Emilio Goeldi, Botany Coordination, Adolpho Ducke Laboratory, 66040-170 Belém, Pará Brazil

[‖]Institute of Exact and Natural Sciences and [⊥]Institute of Biological Sciences, Federal University of Pará, 66075-110 Belém, Pará, Brazil

Ⓢ Supporting Information

ABSTRACT: Odorant-binding proteins (OBPs) are the main olfactory proteins of mosquitoes, and their structures have been widely explored to develop new repellents. In the present study, we combined ligand- and structure-based virtual screening approaches using as a starting point 1633 compounds from 71 botanical families obtained from the Essential Oil Database (EssOilDB). Using as reference the crystallographic structure of N,N-diethyl-meta-toluamide interacting with the OBP1 homo-dimer of Anopheles gambiae (AgamOBP1), we performed a structural and pharmacophoric similarity search to select potential natural products from the library. Thymol acetate, 4-(4-methyl phenyl)-pentanal, thymyl isovalerate, and p-cymen-8-yl demonstrated a favorable chemical correlation with DEET and also had high-affinity interactions with the OBP binding pocket that molecular dynamics simulations showed to be stable. To the best of our knowledge, this is the first study to evaluate on a large scale the potentiality of NPs from essential oils as inhibitors of the mosquito OBP1 using in silico approaches. Our results could facilitate the design of novel repellents with improved selectivity and affinity to the protein binding pocket and can shed light on the mechanism of action of these compounds against insect olfactory recognition.

1. INTRODUCTION

Mosquitoes are the main agents of vector-borne diseases in the tropical regions of the world, causing a high social, economic, and public health impact on these affected regions.[1,2] The disruption of mosquito−human interaction remains one of the most efficient prophylaxis methods against these diseases, and research on chemical repellents against mosquitoes has advanced due to the understanding of mosquito behavior and chemical olfactory receptors.[3−5]

The olfactory system of insects involves diverse trans-membrane odorant receptor proteins located in olfactory membrane neurons, which are expressed in different parts of the insect body.[6] These odorant receptors evolved to respond to several functions in the mosquito life cycle, such as identification of pheromones for reproduction and chemical signals for host recognition.[6−8] The odorant-binding protein 1 (OBP1) is the main olfactory protein involved in the host-seeking mechanism of mosquitoes. The 3D structure of OBP1 is well-conserved across different mosquito species that are vectors of human diseases, such as Aedes aegypti (Protein Data Bank ID: 3K1E),[9] Anopheles gambiae (3V2L and 3R1O),[10] and Culex quinquefasciatus (3OGN),[11] and its structure has been widely investigated for structure-oriented development of novel repellents.[12−14] DEET (N,N-diethyl-meta-toluamide) is one of the most effective, commercially available Food and Drug Administration (FDA)-approved repellents, providing good residual protection against a broad spectrum of insects.[15,16] Its action against OBPs has been extensively investigated as an attractive approach to developing novel bio-inspired repellent compounds by combining ligand- and
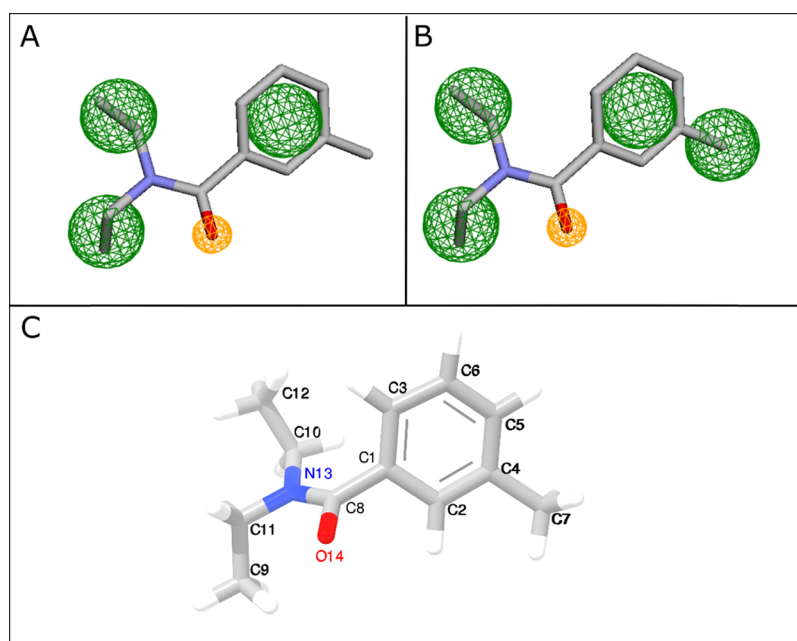
Figure 1. (A, B) Selected pharmacophoric models used to filter the NPs from essential oils. The green circles highlight the aromatic and aliphatic hydrophobic functions, and the orange ones are for the hydrogen-bond acceptor function. (C) Molecular conformer of DEET complexed to *Agam*OBP1.

structure-based approaches.[17,18] However, different studies have reported behavioral insensitivity of different insect species to DEET, which could implicate some inefficiency in its repellency activity.[19−21]

With the increased interest in developing new mosquito repellents from natural products (NPs), essential oils are considered an interesting source due to their widely diverse class of volatile and low-molecular-weight compounds and also to their ovicidal, larvicidal, and repellent activities against human disease vectors.[22−26] With the resurgence of NPs in the development of new bioactive compounds by the pharmaceutical and cosmetic industries[27−30] and due to the cutting-edge technologies of combinatory chemistry, cheminformatics, and molecular modeling, new studies have focused on essential oils to explore their potentiality as mosquito repellents.[23,31,32] Recently, we have used different computational approaches to investigate biomolecular systems with emphasis on enzymatic reaction and inhibition.[33−37] In the present study, using an in silico approach, we performed a comprehensive analysis of the potentiality of 1633 compounds from the essential oils of 71 botanical families deposited in the Essential Oil Database (EssOilDB)[38] by combining a structure- and ligand-based virtual screening, using as reference the structure of DEET complexed to the OBP1 homodimer of *A. gambiae* (*Agam*OBP1). We also investigated the affinity and selectivity of these compounds against *Agam*OBP1 through docking techniques allied with molecular dynamics (MD) simulation and binding free energy calculations.

2. RESULTS AND DISCUSSION

In the present study, we applied a structure- and ligand-based virtual screening approach starting with 1633 compounds from 71 botanical families obtained from the EssOilDB (see the complete list in Table S1). We used as reference the crystallographic structure of DEET interacting with the *Agam*OBP1 homodimer, a relevant odorant protein involved
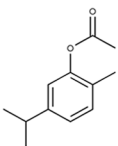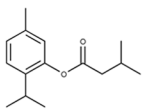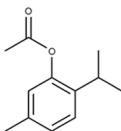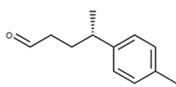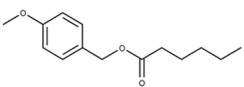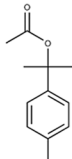
in host-seeking recognition by insects. Using a pharmacophoric prediction and structural similarity search, we analyzed the similarity of these compounds with the reference structure. Then, using docking techniques, MD simulation, and binding free energy calculations, we investigated the potentiality of these compounds as inhibitors of *Agam*OBP1. Our results are further discussed in the following sections.

2.1. Structure-Based Filtering and Similarity Search. A total of 121 compounds from essential oils were obtained after 3D structural similarity filtering using a Tanimoto cutoff of 0.7. After pharmacophoric filtering, 29 compounds were obtained. Two pharmacophoric models were selected: (1) The first model considered the interatomic interactions of the crystallographic structure together with the findings of a previous 3D quantitative structure−activity study of DEET.[4,39] This model comprises one aromatic hydrophobic function located in the aromatic ring, two aliphatic hydrophobic functions at the methyl groups of the diethylamine chain, and one hydrogen-bond acceptor formed by the carboxylic group (Figure 1A). (2) The second model considers the relevance of apolar interactions of DEET in the hydrophobic tunnel and contains an additional aliphatic hydrophobic function formed by the methyl group adjacent to the aromatic ring (Figure 1B). The molecular structure of DEET is shown in Figure 1C.

Based on the physicochemical and structural correlation of the NPs with commercial repellents obtained with PCA, we selected six compounds to determine their selectivity and affinity to the *Agam*OBP1 binding pocket using molecular docking, MD simulation, and binding free energy calculations. The carvacryl acetate and thymol acetate were selected due to their well-known repellent activity against different insect species;[40−43] thus, they could be used for a comparative analysis with the other natural products. The compounds thymyl isovalerate, 4-(4-methylphenyl)-pentanal, and *p*-cymen-8-yl were selected due to their closely physicochemical correlation with commercial repellents DEET and DEPA, as

Table 1. Selected NPs from Essential Oils To Investigate Their Affinity against *Agam*OBP1 Binding Pocket[a]

Structure	Common name	Chemical Class	Tanimoto 3D value	RMSD value (Å)	Origin Species
	carvacryl acetate	Monoterpenoid	0.71	0.69	*Valeriana officinalis Ageratum conyzoides Thymus munbyanus*
	thymyl isovalerate	Sesquiterpenoid	0.78	0.63	*Eupatorium cannabinum Valeriana alpestris*
	thymol acetate	Monoterpenoid	0.79	0.67	*Aeollanthus pubescens Caryopteris odorata Lippia gracillis*
	4-(4-methylphenyl)-pentanal	Phenylpropanoid	0.80	0.62	*Santalum spicatum*
	p-anisyl hexanoate	Phenylpropanoid	0.81	0.77	*Heracleum paphlagonicum*
	p-cymen-8-yl	Monoterpenoid	0.80	0.62	*Pituranthos scoparius Chukrasia tabularis*

[a]The compounds are identified by molecular structure, common name, chemical class, structural similarity to DEET (Tanimoto 3D value and RMSD), and some origin species.

shown by the PCA plot, and the *p*-anisyl hexanoate was selected due to its structural and pharmacophoric similarities to crystallographic DEET. The common name, chemical class, structural similarity (RMSD and Tanimoto 3D), and some origin species of the selected compounds are shown in Table 1.

The compounds *p*-cymen-8-yl, thymol acetate, carvacryl acetate, 4-(4-methylphenyl)-pentanal, thymyl isovalerate, and *p*-anisyl hexanoate showed satisfactory structural similarity with DEET according to the following Tanimoto 3D values: 0.80, 0.79, 0.71, 0.80, 0.78, and 0.81, respectively. Supporting this structural similarity, *p*-cymen-8-yl, thymol acetate, carvacryl acetate, 4-(4-methylphenyl)-pentanal, and thymyl isovalerate also exhibited a favorable physicochemical correlation with commercial repellents. Figure 2 depicts the

PCA scatter plot; the first circle highlights the correspondence between the NPs 2-methoxy-4,5-methylenedioxypropiophenone, methyl *N*-methylanthranilate, and (*S*)-1-(4-acetoxyphenyl)propyl acetate with the repellents dimethyl phthalate (DBP), methylanthranilate, and 3-cyclohexyl propanoic acid. The second circle highlights the chemical correspondence between NPs thymol acetate, carvacryl acetate, 4-(4-methyl phenyl)-pentanal, benzyl (2*S*)-2-methylbutanoate, thymyl isovalerate, and *p*-cymen-8-yl with the commercial repellents *N,N*-diethyl phenylacetamide (DEPA) and DEET. We obtained the following variance percentage for the principal components: 44.22% (PC1), 26.10% (PC2), and 16.79% (PC3). The raw data of compound properties (NPs
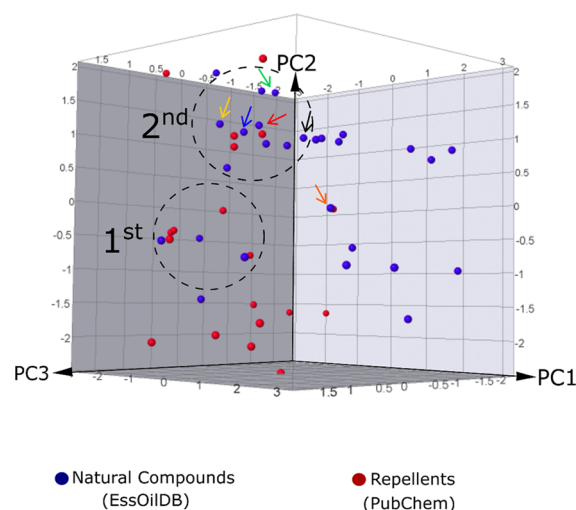
Figure 2. Scatter plot showing the chemical space of the NPs and the commercially used repellents. The x, y, and z axes exhibit the contribution of each principal component for the chemical profile of the compounds. The selected compounds are identified by color arrows: p-cymen-8-yl (blue), thymol acetate (red), carvacryl acetate (yellow), and 4-(4-methylphenyl)-pentanal (green), thymyl isovalerate (black), and p-anisyl hexanoate (orange).

and repellents) used to calculate the PCA is available in Table S2.

Interestingly, several studies have highlighted the repellent activity of thymol and thymol acetate against different insects, which are vectors of diseases such as *Ixodes ricinus* (Acari: Ixodidae),[40] *Anopheles subpictus* Grassi, *Anopheles stephensi*

(Diptera: Culicidae),[42,44] *Culex pipiens* (Diptera: Culicidae),[41] and crop pests such as *Meligethes aeneus* (Fabricius) (Coleoptera: Nitidulidae).[31] Similarly, carvacryl acetate, a monoterpene derivative of carvacrol found in a high percentage in the essential oils of some Lamiaceae species such as *Clinopodium* sp.[45] and *Thymus* sp.,[46] has a well-reported insecticidal and oviposition deterrence against different insect species.[54,55] In addition, p-cymen-8-ol has a high repellent activity against *Lasioderma serricorne* Fabricius (Coleoptera: Anobiidae),[47,48] and its derivative molecule p-cymene was used against *A. gambiae*.[49]

Several studies have reported the specific inhibitory activity of some NPs from essential oil against insect OBPs with satisfactory binding affinity, such as sesquiterpenes (e.g., benzaldehyde, β-myrcene, and α-copaene)[13] and alcohols (e.g., n-decanol and n-dodecanol).[12] In the present study, we identified that predominantly monoterpenoids, such as p-cymen-8-yl, thymol acetate, and carvacryl acetate, mimic the binding mode of DEET, exhibiting similar pharmacophoric groups and intermolecular interactions with the protein pocket, which sheds light on the molecular mechanism of action of these compounds against olfactory recognition of insects, reinforcing the previous experimental repellency studies for this chemical class.[40,41,48,50]

2.2. Interactions of NPs with the *Agam*OBP1 Binding Pocket. The *Agam*OBP1 structure is composed of two monomers, each consisting of six α-helices, with the odorant-binding pocket located at the center of a hydrophobic tunnel through the dimeric interface.[39,51] The crystallographic structure of *Agam*OBP1 bound to DEET reveals that the binding pocket cavity is formed by the residues Leu80, Leu73,

Figure 3. Superposition of the average structure obtained from MD simulation of each NP and the docked DEET with the crystallographic structure: (A) p-cymen-8-yl, (B) 4-(4-methylphenyl)-pentanal, (C) p-anisyl hexanoate, (D) docked DEET, (E) thymyl isovalerate, (F) carvacryl acetate, (G) thymol acetate. Crystallographic DEET (PDB: 3N7H) is shown in light blue, the residues are in green, and the docked ligands are in gray. Residues from chain B are indicated with a prime (′).

Figure 4. Noncovalent interactions of the selected NPs against the *Agam*OBP1 binding pocket: (A) 4-(4-methylphenyl)-pentanal, (B) thymol acetate, (C) thymyl isovalerate, (D) carvacryl acetate, (E) *p*-cymen-8-yl, (F) *p*-anisyl hexanoate. Residues from chain B are indicated with a prime (′).

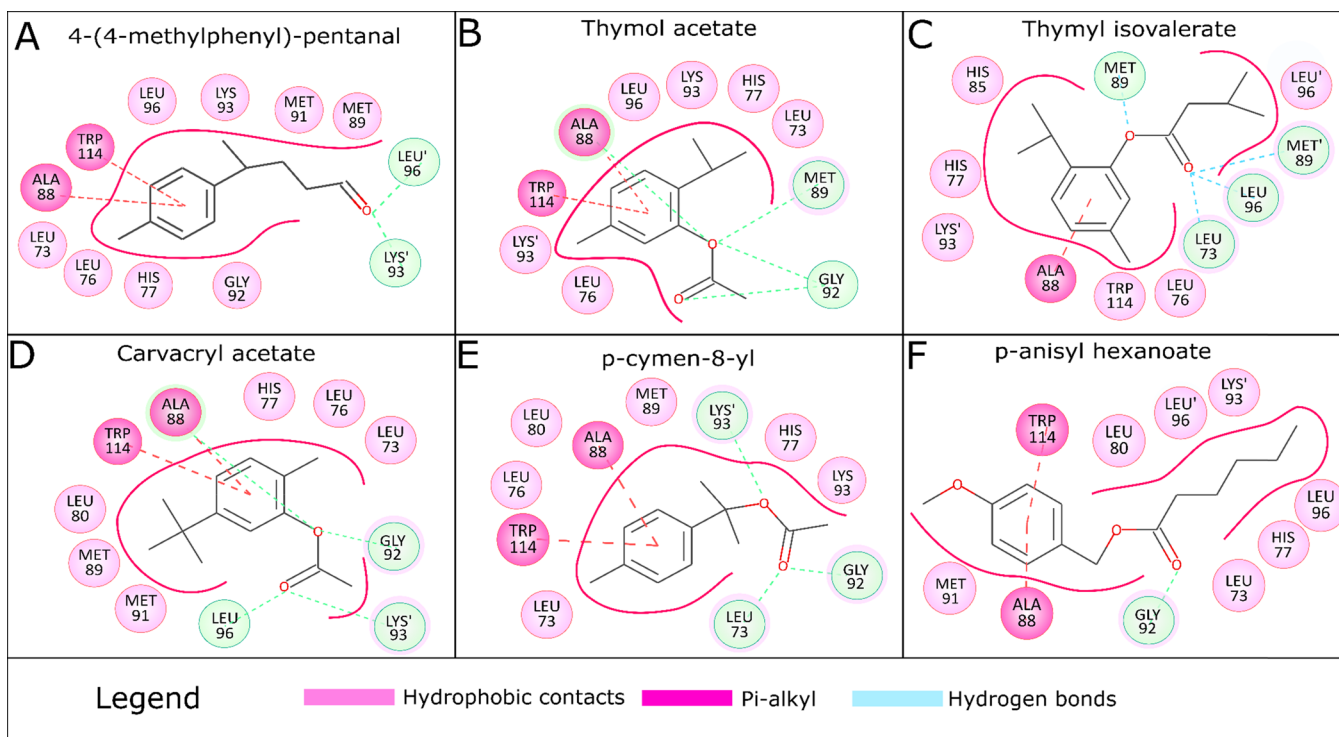Leu76, and His77 (α-helix 4); Met91, Ala88, Met89, and Gly92 (α-helix 5); and Trp114 (α-helix 6); also, the residues Leu96, Lys930, Arg940, and Leu960 and the two molecules of DEET bound to the dimeric interface of *Agam*OBP1 interact with each other by the methyl carbon atoms. In addition, studies have demonstrated that odorant molecules could interact in several locations of the OBP binding pockets with partial occupancies, that is, in the central cavity of the monomeric subunit as well as to the OBP dimeric interface.[52−54] Based on these results, we selected for docking analyses the dimeric interface of the DEET-binding pocket located between the two monomers, which is formed by the residues of the helices α4, α5, and α6 (intermolecular interactions and atomic distances obtained in docking are available in Table S3).

The noncovalent interactions formed between the *Agam*OBP1 binding pocket and the NPs were analyzed over 10 ns of MD simulation. The selected NPs formed numerous hydrophobic interactions with the *Agam*OBP1 binding pocket, with residues Leu76, His77, Met89, Leu96, and Trp114 repeating interactions similar to those observed with the crystallographic structure of DEET. *Agam*OBP1 residues Ala88 and Trp114 formed π−alkyl interactions with the aromatic ring of the selected compounds, and some residues, such as Gly92, Leu73, and Met89 (chain A) as well as Lys93 and Leu96 (chain B), formed hydrogen bonds with the oxygenated groups (see Table S4). We also noted that water molecules interact with DEET, with the residues located in the binding pocket, such as Trp114, Asp78, Gly92, and Ser79, and with the main chain of residues Cys95 and Gly92.

An overview of the intermolecular interactions formed between the residues of the *Agam*OBP1 binging pocket and the selected NPs and docked DEET is shown in Figure 3 and

compared with a structural superposition with the crystallographic DEET. The diagram showing the interactions of the six NPs with the *Agam*OBP1 binding pocket over 10 ns of MD simulation is shown in Figure 4. Thus, we then performed binding energy calculations to analyze the binding affinities of the selected NPs complexed to the *Agam*OBP1 pocket.

2.3. Conformational Stability of the *Agam*OBP1− Ligand Complexes and the Binding Affinities of the Natural Products. The conformational stability of *Agam*OBP1 bound and unbound to the ligands over 100 ns of MD simulation is shown by the RMSD plots (Figure 5). We observed that the *Agam*OBP1 heterodimer complexed with the ligands reached equilibrium at 70 ns of MD simulation, exhibiting the following average RMSD values: 1.45 ± 0.21 Å (complexed with DEET), 1.74 ± 0.29 Å (complexed with thymol acetate), 1.74 ± 0.32 Å (thymyl isovalerate), 1.61 ± 0.23 Å (carvacryl acetate), 1.43 ± 0.20 Å (*p*-cymen-8-yl), 1.93 ± 0.43 Å (*p*-anisyl hexanoate), and 1.49 ± 0.21 Å (4-(4-methylphenyl)-pentanal). Corroborating these results, the RMSD plot of the NP structures exhibited stability over the simulations and indicated a favorable interaction with the *Agam*OBP1 binding pocket, which is also observed for the DEET structure (Figure S1).

During the first MD simulation of the *Agam*OBP1-DEET complex (positive control), we noted that the protein structure undergoes a conformational change at 60 ns, which can be seen by the RMSD values with a deviation of 3.0 Å (see Figure S2 for triplicate MD simulation of the *Agam*OBP1−DEET complex). These increased RMSD values could be explained by the movement of a loop segment located in the N-terminal region. Using structural superposition (Figure S3A,B), we analyzed the conformations of the *Agam*OBP1−DEET complex before (60 ns, yellow color) and after (70 ns, blue
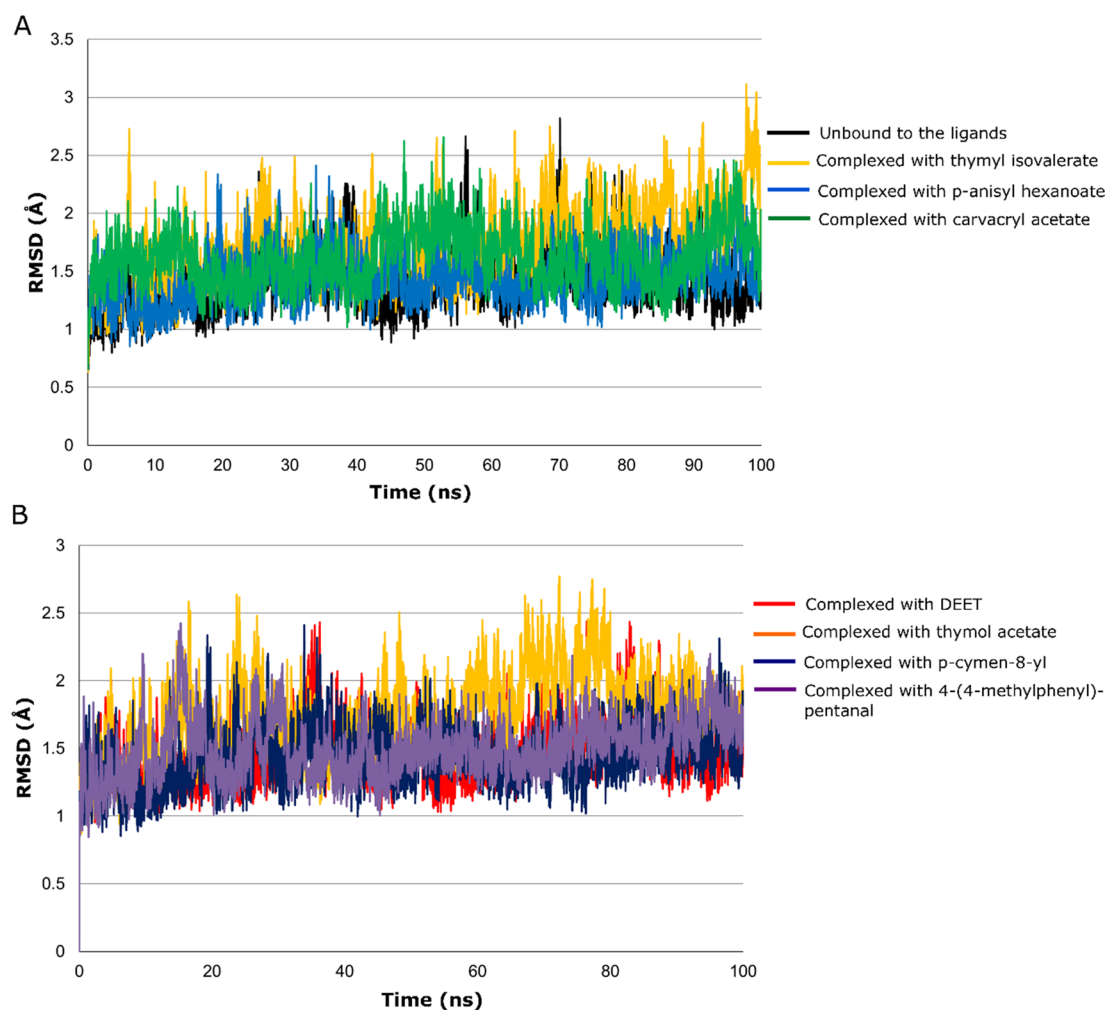
Figure 5. RMSD plots of the *Agam*OBP1 structure bound and unbound to the ligands obtained over 100 ns of MD simulation. (A) *Agam*OBP1 unbound to the ligands (black), OBP1 complexed with thymyl isovalerate (yellow), *p*-anisyl hexanoate (blue), and carvacryl acetate (green). (B) *Agam*OBP1 complexed with DEET (red), thymol acetate (yellow), *p*-cymen-8-yl (blue), and 4-(4-methyl phenyl)-pentanal (purple).

color) the increased RMSD values, and we noted that the protein structure maintains slight deviations in its conformation, except for a loop segment (L1) located at the N-terminal region. The loop segment L1 moves toward the α-helix, leading to the formation of intermolecular interactions that stabilize the whole protein structure (Figure S3 C). The conformational changes in the loop do not alter the *Agam*OBP1 active site, and the DEET structure maintains a stable interaction with residues of the binding site.

In the present study, we calculate the binding free energy using SIE method.[55] As seen from computational binding results, thymyl isovalerate (-7.34 ± 0.09 kcal mol^{-1}), *p*-anisyl hexanoate (-6.85 ± 0.10 kcal mol^{-1}), and 4-(4-methylphenyl)-pentanal (-6.81 ± 0.08 kcal mol^{-1}) are the most efficient inhibitors of the OBP1 odorant pocket followed by *p*-cymen-8-yl, carvacryl acetate, and thymol acetate (Table 2 and Table S5). Note that we have used PCA for analyzing the convergent trajectories and selected the time interval for the binding free energy calculation. The analysis of convergent trajectories for each complex studied over the 100 ns of MD is depicted in Figure S4. It is also worth noting that a previous study obtained similar results using docking energies for DEET ($\Delta G = -5.86$ kcal mol^{-1}; $K_i = 50.51$ μM) and potential repellents of *Agam*OBP1, such as 2-methyl-1-(1-oxodecyl)piperidine

Table 2. Predicted Binding Free Energies Calculated by SIE of the Selected NPs from Essential Oil with the *Agam*OBP1 Binding Pocket

compounds	ΔG_{SIE} (kcal mol^{-1})
DEET	-6.85 ± 0.13
carvacryl acetate	-6.76 ± 0.12
thymyl isovalerate	-7.34 ± 0.09
thymol acetate	-6.66 ± 0.07
4-(4-methylphenyl)-pentanal	-6.81 ± 0.08
p-anisyl hexanoate	-6.85 ± 0.10
p-cymen-8-yl	-6.75 ± 0.10

($\Delta G = -7.36$ kcal mol^{-1}; $K_i = 4.04$ μM), 1-(1-oxoundecyl)-piperidine ($\Delta G = -7.20$ kcal mol^{-1}; $K_i = 5.28$ μM), and *N,N*-diethyl-3-phenylpropanamide ($\Delta G = -6.49$ kcal mol^{-1}; $K_i = 17.21$ μM).[39] Similarly, a previous study performed binding free energy calculations using the MM/GBSA method for β-caryophyllene (sesquiterpene), β-myrcene (monoterpene), and *cis*-β-ocimene (monoterpene) complexed to different OBP classes of *Hydroides elegans*, and their energy values approximated our calculated values of OBP1,[13] which is also consistent with the inhibitory activity.

The crystallographic structure of *Agam*OBP1 complexed with DEET reveals that the majority of residues located at
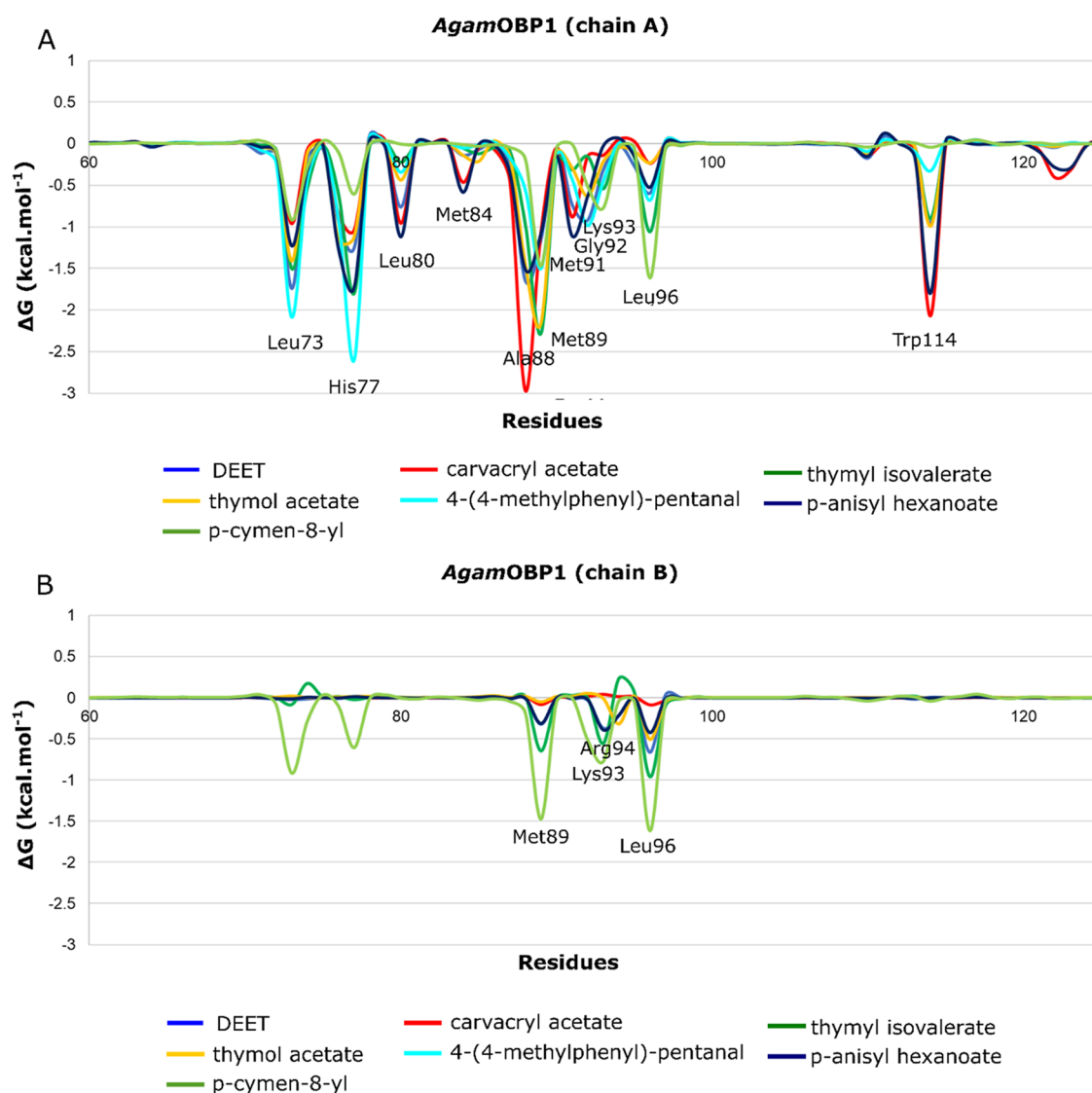
Figure 6. Ligand pairwise per-residue energy decomposition analysis of *Agam*OBP1 binding pocket. ΔG values of (A) *Agam*OBP1 chain A and (B) *Agam*OBP1 chain B: DEET (blue), thymol acetate (yellow), *p*-cymen-8-yl (light green), carvacryl acetate (red), 4-(4-methylphenyl)-pentanal (cyan), thymyl isovalerate (green), and *p*-anisyl hexanoate (dark blue).

chain A, such as Leu73, Leu76, His77, Ala88, Met91, Gly92, Lys93, and Leu96, form hydrophobic contacts with the ligands.[39] In the present study, we noted that the NPs also showed a similar binding mode, and the residues Leu73, His77, Leu80, Ala88, Gly92, Leu96, and Trp144 exhibited the most energetic contribution for ligand stabilization in the *Agam*OBP1 binding pocket (Figure 6). In contrast, the residues of *Agam*OBP1 chain B exhibited a minor contribution to ligand stabilization, and we noted a special interaction with Met89, Lys93, and Leu96 that was revealed as the most important to ligand binding.

Structural waters have been reported as relevant for the binding stability of OBP-odorant molecules and to the OBP recognition process.[39] Our analyses identified that water molecules interact with DEET (DEET-C1 with Wat1815-O; average distance: 4.06 ± 0.20 Å) and with the side chains of residues located in the binding pocket, Trp114 (occupancy: 77.60%, Trp114-NE1 atom with Wat1815-O; average distance: 1.97 ± 0.15 Å), and minor interactions were noted for the residues Asp78 (occupancy: 0.25%), Gly92 (0.15%), and Ser79

(0.20%) and with the main chain of the residues Cys95 (3.65%) and Gly92 (0.10%). These interactions with water molecules are consistent with the crystallographic findings. Considering the NPs, we do not note H-bond interactions with water molecules, but similar interactions occurred with residues of the *Agam*OBP1 binding pocket when bound to thymol acetate, *p*-anisyl hexanoate, and thymyl isovalerate. The non-occurrence of interactions between water molecules and ligands could be explained by the different occupancies formed by these NPs in the *Agam*OBP1 binding pocket, which fill the same space previously occupied by the water.

Our results revealed new structural insights about the mechanism of action of these volatile compounds sourced from aromatic plants against the olfactory recognition of mosquitoes, and the findings indicate that the structures of these NPs could be further validated against *Agam*OBP1.

3. CONCLUSIONS

We have demonstrated that NPs from essential oils, such as thymyl isovalerate, thymol acetate, *p*-anisyl hexanoate, and *p*-

cymen-8-yl, mimic the binding mode of DEET, a well-known repellent, forming hydrophobic and H-bond interactions with the *Agam*OBP1 binding pocket. Our results are supported by computational evidence, such as (1) structural, pharmacophoric, and binding mode similarity of these compounds with that of DEET as verified through structural alignment, pharmacophoric prediction, and molecular docking; (2) high conformational stability of these compounds in the OBP1 binding pocket as analyzed through MD simulations; and (3) high predicted binding affinity of the NPs when compared with the DEET−OBP1 complex as revealed by crystallographic structure. We also found that thymol acetate, 4-(4-methyl phenyl)-pentanal, thymyl isovalerate, and *p*-cymen-8-yl share similar physicochemical properties with the commercial repellents DEPA and DEET. Considering that computational methods have been a cost-effective and predictive approach for analyzing the binding affinity of olfactory receptors with the odorant molecules[7,56] and that they have consequently been applied to the identification of novel potential repellents against different insect species,[57] our findings reinforce the potentiality of NPs as an interesting source for the development of novel mosquito repellents. Further experimental studies should be performed with the compounds *p*-anisyl hexanoate and 4-(4-methyl phenyl)-pentanal.

4. MATERIALS AND METHODS

An overview of the structure- and ligand-based virtual screening methodology applied in the present study is shown in Figure 7 and described in detail in the sections below.

4.1. Search for 3D Structural Similarity. First, we analyzed the structural similarity of the NPs from essential oils

Essential Oil Database
1,633 compounds from 74 botanical families

3D Structural Similarity Screening
Comparison with DEET conformer

Pharmacophoric Screening
Comparison with DEET complexed to OBP1

Analysis of Chemical Space
Principal Component Analysis
Repellents vs Natural Products

Analysis of Target Inhibition
1. Molecular Docking
2. Molecular Dynamics Simulation
3. Binding Free Energy Calculations

Figure 7. Overview of the applied computational methodology.

with the DEET crystallographic conformer using Screen3D (ChemAxon).[58] A Tanimoto coefficient cutoff value of 0.7 was applied as a measure of 3D similarity for selecting similar compounds from the initial library with 1633 compounds from the EssOilDB.[38] Screen3D automatically generated the 3D conformers; thus, we limited the maximum number of conformers per compound to 4. The Tanimoto coefficient cutoff is defined by eq 1.[59]

$$s_{A,B} = \frac{\left[\sum_{J=1}^{n} x_{JA}x_{JB}\right]}{\left[\sum_{J=1}^{n} (x_{JA})^2 + \sum_{J=1}^{n} (x_{JB})^2 - \sum_{J=1}^{n} x_{JA}x_{JB}\right]} \quad (1)$$

Here, $s_{A,B}$ denotes the similarity between both compounds (A and B), x_{JA} means the jth features of compound A, x_{JB} represents the jth features of compound B, and $x_{JA}x_{JB}$ is the feature present in both analyzed compounds.

4.2. Pharmacophoric Prediction and Filtering. Next, we used the Pharmit server to screen the NP structures with similar pharmacophoric groups and shape with the DEET conformer complexed to *Agam*OBP1 (PDB: 3N7H, X-ray structure, resolution: 1.6 Å).[60] We analyzed the superposition of the predicted pharmacophores of the natural compound with two pharmacophoric models of DEET complexed with the *Agam*OBP1 homodimer. Based on these initial screenings, six compounds were selected for further analysis.

4.3. Molecular Docking. The Molegro Virtual Docker (MVD) program, which uses the evolutionary algorithm MolDock,[61] was used to perform molecular docking simulations to analyze the binding mode of the NPs complexed to the *Agam*OBP1 homodimer. First, to validate the docking protocol, redocking simulations were performed with the DEET structure against the *Agam*OBP1 homodimer. Root-mean-square deviation (RMSD) values less than or equal to 1.0 Å were considered satisfactory for replicating the ligand binding mode in the crystallographic structure. Next, for the docking simulations, docking grids with radii of 8 to 15 Å, depending on the selected ligand, were positioned in the *Agam*OBP1 active site between both *Agam*OBP1 monomers using the spatial coordinates of crystallographic DEET as a reference. Water molecules, ions, and the DEET structure were removed from both OBP1 chains before the docking simulations. Then, we performed the flexible docking protocol of MVD, which consider the flexibility of the ligand and residue side chains.[62] All poses obtained were ranked according to the best superposition with the crystallographic structure of DEET and lower docking energy.

4.4. Molecular Dynamics Simulation and Analysis of the *Agam*OBP1−Ligand Complexes. Using the Amber16 package,[63] MD simulations were performed for the following *Agam*OBP1 systems: (1) *Agam*OBP1 unbound to the ligands (ligand-free), (2) *Agam*OBP1 complexed with DEET (PDB: 3N7H), and (3) the six selected NPs from essential oils. First, the partial atomic charges of the ligands were determined using the restrained electrostatic potential (RESP) protocol[64] through quantum mechanical calculations carried out in the Gaussian 09 program.[65] using the Hartree−Fock method[66] with the 6-31G* basis set.[67] The biomolecular systems were solvated in the tLeap module using an octahedral truncated water box with TIP3P, an explicit solvation model.[68] The distance between the water box wall and the atoms of the solvated system was set to 12 Å. Na⁺ counterions were added to the water box to maintain electroneutrality. The force fields
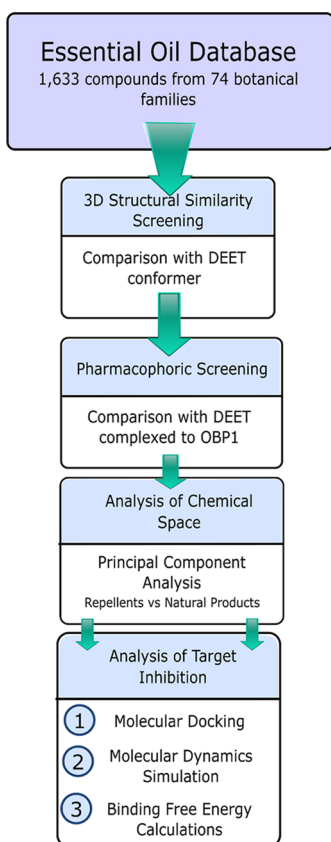
ff14SB[69] and General Amber Force Field[70] were used to parameterize the protein (*Agam*OBP1) and the ligand structures (NPs and DEET), respectively. An energy minimization protocol with six steps that included the steepest-descent and conjugated gradient algorithm was performed for all systems. All hydrogen atoms, water, and ions were minimized by 10,000 cycles for each step followed by minimization of the whole *Agam*OBP1 system with the progressive decrease of restraints. Next, the whole system was heated through 10 heating steps. The first heating step was performed at a constant volume for 20 ps, increasing the temperature to 100 K. From the second to the ninth step, 1 ns was used to raise the temperature gradually from 100 to 275 K. In the 10th heating step, the temperature reached 300 K, which was then maintained using 5 ns of MD simulation to equilibrate the density at constant pressure (1 bar). The temperature was maintained at 300 K by coupling to a Langevin thermostat using a collision frequency of 2 ps^{-1}, and the constant isotropic pressure was maintained at 1 bar by using the Berendsen barostat. All stages of the simulations employed a cutoff of 10 Å for nonbonded interactions, and the particle mesh Ewald (PME) method was used to compute the long-range electrostatic interactions. The SHAKE algorithm was applied for all H bonds during MD simulation, and the time step was set to 2 fs.[71] Finally, MD simulation was performed in 100 ns. The RMSD plot was obtained for each system during the simulation using the heavy atoms of the protein backbone. The noncovalent interactions of the receptor–ligand complex were analyzed over 10 ns of MD simulation using PyContact[72] and visually inspected using the Visual Molecular Dynamics (VMD) program.[73]

4.5. Analysis of Conformational States over the MD Simulation. To calculate the binding free energy and to measure the molecular interactions between the ligands and *Agam*OBP1 binding pocket, we selected the intervals of the MD trajectories based on the convergent conformational states of *Agam*OBP1–ligand complexes obtained during 100 ns of MD simulation using principal component analysis (PCA). PCA is a transformation technique that converts a series of potentially coordinated observations present in a covariance matrix, reducing the linear correlations among them, thus transforming into a set of orthogonal vectors named principal components (PCs).[74] The first component (PC1) maximizes the variance data in the data set and the rest of the variance is represented by the second (PC2) and third component (PC3), respectively. The PCA combined with MD simulations of proteins has been widely applied to analyze the local and collective movements of protein structures,[75,76] to determine the conformational changes that favor enzyme catalysis,[77] to explore the functional roles of ion binding in protein structure,[78] and to sample the convergence and correspondence between the protein structures over the MD simulation.[79] Our conformational analyses were performed in the CPPTRAJ[80] and Bio3D[81] programs, and the scatter plots were build using PC1 and PC2.

4.6. Binding Free Energy Calculations. To compute the binding free energy between the ligands (NPs and DEET) and the *Agam*OBP1 structure, we selected three intervals with 1000 frames from each MD trajectory. To calculate the binding free energy, we applied the solvated interaction energy (SIE) method[55] available in SIETRAJ.[82] We also performed a ligand pairwise per-residue energy decomposition analysis using the molecular mechanics/generalized Born surface area (MM/GBSA) method[83] available in Amber16.[63]

4.7. Analysis of the Chemical Space of Natural Products from Essential Oils. To analyze the chemical space of the filtered NPs obtained from essential oils, we compared them with 18 approved or experimental repellents (Table S6) using PCA. Six physicochemical and structural descriptors were used in PCA: number of rotatable bonds, *c* log *P*, molecular weight, number of H bond donors, H bond acceptors, and number of aromatic rings. These descriptors have been applied to determine the herbicide-, fungicide-, pesticide-, and insecticide-likeness of compounds.[84] All properties were calculated using the Instant JChem suite.[58]

■ ASSOCIATED CONTENT

Ⓢ Supporting Information

The Supporting Information is available free of charge at https://pubs.acs.org/doi/10.1021/acsomega.9b03157.

> RMSD plots of the analyzed natural products from essential oils and the reference structure (DEET) obtained over 100 ns of MD simulation (Figure S1); RMSD plots of *Agam*OBP1 structure complexed with DEET analyzed in triplicate MD simulation (Figure S2); structural superposition of the *Agam*OBP1-DEET complex before and after the conformational changes (Figure S3); and analysis of convergent trajectories of *Agam*OBP1 complexes analyzed over the 100 ns of MD simulation shown in the free energy principal component analysis (PC1 vs PC2) (Figure S4) (PDF)

> Complete list of NPs from essential oils identified by their respective molecular structure, common name, SMILE code, and molecular weight (Table S1) (ZIP)

> Complete raw data of compounds properties used to calculate the PCA (Table S2) (ZIP)

> Interatomic interactions types and atomic distances between the ligands and the residue side chains of the *Agam*OBP1 binding pocket obtained in molecular docking (Table S3) (XLSX)

> Analysis of noncovalent interactions between the NPs and *Agam*OBP1 binding pocket obtained over 10 ns of MD simulation (Table S4) (ZIP)

> Energy values calculated using the SIE method for the three selected intervals of MD simulation (Table S5) (XSLX)

> Chemical structure, common name, molecular formula PubChem CID, and physicochemical and structural properties (*c* log *P*, molecular weight, H-bond donors, H-bond acceptors, number of aromatic rings, and rotatable bonds) of the selected commercial repellents (Table S6) (XSLX)

■ AUTHOR INFORMATION

Corresponding Authors
*E-mail: kaue.costa@ufopa.edu.br. Phone: +55 93 2101-6771 (K.S.D.C.).
*E-mail: lameira@ufpa.br (J.L.).

ORCID Ⓘ
Kauê Santana da Costa: 0000-0002-2735-8016
Jorddy Neves Cruz: 0000-0003-0529-3714
Claudio Nahum Alves: 0000-0001-6576-4229

Notes

The authors declare no competing financial interest.

■ REFERENCES

(1) Rascalou, G.; Pontier, D.; Menu, F.; Gourbière, S. Emergence and Prevalence of Human Vector-Borne Diseases in Sink Vector Populations. *PLoS One* 2012, 7, No. e36858.

(2) Valenzuela, J. G.; Aksoy, S. Impact of Vector Biology Research on Old and Emerging Neglected Tropical Diseases. *PLoS Neglected Trop. Dis.* 2018, 12, No. e0006365.

(3) Paluch, G.; Bartholomay, L.; Coats, J. Mosquito Repellents: A Review of Chemical Structure Diversity and Olfaction. *Pest Manage. Sci.* 2010, 66, 925−935.

(4) Bhattacharjee, A. K.; Dheranetra, W.; Nichols, D. A.; Gupta, R. K. 3D Pharmacophore Model for Insect Repellent Activity and Discovery of New Repellent Candidates. *QSAR Comb. Sci.* 2005, 24, 593−602.

(5) Devillers, J. 2D and 3D Structure−Activity Modelling of Mosquito Repellents: A Review. *SAR QSAR Environ. Res.* 2018, 29, 693−723.

(6) Zheng, W.; Peng, W.; Zhu, C.; Zhang, Q.; Saccone, G.; Zhang, H. Identification and Expression Profile Analysis of Odorant Binding Proteins in the Oriental Fruit Fly Bactrocera Dorsalis. *Int. J. Mol. Sci.* 2013, 14, 14936−14949.

(7) Boyle, S. M.; McInally, S.; Ray, A. Expanding the Olfactory Code by in Silico Decoding of Odor-Receptor Chemical Space. *Elife* 2013, 2, No. e01120.

(8) Zhang, Y.; Ren, Y.; Wang, X.; Liu, Y.; Wang, N. Responses to Host Plant Volatiles and Identification of Odorant Binding Protein and Chemosensory Protein Genes in Bradysia Odoriphaga. *ACS Omega* 2019, 4, 3800−3811.

(9) Leite, N. R.; Krogh, R.; Xu, W.; Ishida, Y.; Iulek, J.; Leal, W. S.; Oliva, G. Structure of an Odorant-Binding Protein from the Mosquito Aedes Aegypti Suggests a Binding Pocket Covered by a PH-Sensitive "Lid". *PLoS One* 2009, 4, No. e8006.

(10) Lagarde, A.; Spinelli, S.; Tegoni, M.; He, X.; Field, L.; Zhou, J.-J.; Cambillau, C. The Crystal Structure of Odorant Binding Protein 7 from Anopheles Gambiae Exhibits an Outstanding Adaptability of Its Binding Site. *J. Mol. Biol.* 2011, 414, 401−412.

(11) Mao, Y.; Xu, X.; Xu, W.; Ishida, Y.; Leal, W. S.; Ames, J. B.; Clardy, J. Crystal and Solution Structures of an Odorant-Binding Protein from the Southern House Mosquito Complexed with an Oviposition Pheromone. *Proc. Natl. Acad. Sci. U. S. A.* 2010, 107, 19102−19107.

(12) Bezerra-Silva, P. C.; Dutra, K. A.; Santos, G. K. N.; Silva, R. C. S.; Iulek, J.; Milet-Pinheiro, P.; Navarro, D. M. A. F. Evaluation of the Activity of the Essential Oil from an Ornamental Flower against Aedes Aegypti: Electrophysiology, Molecular Dynamics and Behavioral Assays. *PLoS One* 2016, 11, No. e0150008.

(13) González-González, A.; Palma-Millanao, R.; Yáñez, O.; Rojas, M.; Mutis, A.; Venthur, H.; Quiroz, A.; Ramírez, C. C. Virtual Screening of Plant Volatile Compounds Reveals a High Affinity of *Hylamorpha Elegans* (Coleoptera: Scarabaeidae) Odorant-Binding Proteins for Sesquiterpenes from Its Native Host. *J. Insect Sci.* 2016, 16, 30.

(14) Venthur, H.; Zhou, J.-J. Odorant Receptors and Odorant-Binding Proteins as Insect Pest Control Targets: A Comparative Analysis. *Front. Physiol.* 2018, 9, 1163.

(15) Syed, Z.; Leal, W. S. Mosquitoes Smell and Avoid the Insect Repellent DEET. *Proc. Natl. Acad. Sci. U. S. A.* 2008, 105, 13598−13603.

(16) Alzogaray, R. A.; Fontan, A.; Zerba, E. N. Repellency of Deet to Nymphs of Triatoma Infestans. *Med. Vet. Entomol.* 2000, 14, 6−10.

(17) Thireou, T.; Kythreoti, G.; Tsitsanou, K. E.; Koussis, K.; Drakou, C. E.; Kinnersley, J.; Kröber, T.; Guerin, P. M.; Zhou, J. J.; Iatrou, K.; et al. Identification of Novel Bioinspired Synthetic Mosquito Repellents by Combined Ligand-Based Screening and OBP-Structure-Based Molecular Docking. *Insect Biochem. Mol. Biol.* 2018, 98, 48−61.

(18) Murphy, E. J.; Booth, J. C.; Davrazou, F.; Port, A. M.; Jones, D. N. M. Interactions of Anopheles Gambiae Odorant-Binding Proteins with a Human-Derived Repellent: Implications for the Mode of Action of N,N-Diethyl-3-Methylbenzamide (DEET). *J. Biol. Chem.* 2013, 288, 4475−4485.

(19) Sfara, V.; Mougabure-Cueto, G.; Zerba, E. N.; Alzogaray, R. A. Adaptation of the Repellency Response to DEET in Rhodnius Prolixus. *J. Insect Physiol.* 2011, 57, 1431−1436.

(20) Stanczyk, N. M.; Brookfield, J. F. Y.; Ignell, R.; Logan, J. G.; Field, L. M. Behavioral Insensitivity to DEET in Aedes Aegypti Is a Genetically Determined Trait Residing in Changes in Sensillum Function. *Proc. Natl. Acad. Sci. U. S. A.* 2010, 107, 8575−8580.

(21) Stanczyk, N. M.; Brookfield, J. F. Y.; Field, L. M.; Logan, J. G. Aedes Aegypti Mosquitoes Exhibit Decreased Repellency by DEET Following Previous Exposure. *PLoS One* 2013, 8, No. e54438.

(22) Ma, L.; Zhang, Z.; Liu, Z.; Pan, Q.; Wang, J.; Li, X.; Guo, F.; Liang, C.; Hu, L.; Zhou, J.; et al. Identification of Small Molecule Compounds Targeting the Interaction of HIV-1 Vif and Human APOBEC3G by Virtual Screening and Biological Evaluation. *Sci. Rep.* 2018, 8, 8067.

(23) Bertoli, A.; Conti, B.; Mazzoni, V.; Meini, L.; Pistelli, L. Volatile Chemical Composition and Bioactivity of Six Essential Oils against the Stored Food InsectSitophilus ZeamaisMotsch. (Coleoptera Dryophthoridae). *Nat. Prod. Res.* 2012, 26, 2063−2071.

(24) Regnault-Roger, C.; Vincent, C.; Arnason, J. T. Essential Oils in Insect Control: Low-Risk Products in a High-Stakes World. *Annu. Rev. Entomol.* 2012, 57, 405−424.

(25) Zhao, M.; Liu, Q.; Liu, Q.; Liu, Z. Identification of Larvicidal Constituents of the Essential Oil of Echinops Grijsii Roots against the Three Species of Mosquitoes. *Molecules* 2017, 22, 205.

(26) Yu, K.-X.; Wong, C.-L.; Ahmad, R.; Jantan, I. Mosquitocidal and Oviposition Repellent Activities of the Extracts of Seaweed Bryopsis Pennata on Aedes Aegypti and Aedes Albopictus. *Molecules* 2015, 20, 14082−14102.

(27) Thomford, N.; Senthebane, D.; Rowe, A.; Munro, D.; Seele, P.; Maroyi, A.; Dzobo, K. Natural Products for Drug Discovery in the 21st Century: Innovations for Novel Drug Discovery. *Int. J. Mol. Sci.* 2018, 19, 1578.

(28) Galúcio, J. M.; Monteiro, E. F.; de Jesus, D. A.; Costa, C. H.; Siqueira, R. C.; dos Santos, G. B.; Lameira, J.; da Costa, K. S. In Silico Identification of Natural Products with Anticancer Activity Using a Chemo-Structural Database of Brazilian Biodiversity. *Comput. Biol. Chem.* 2019, 83, 107102.

(29) Li, F.; Wang, Y.; Li, D.; Chen, Y.; Dou, Q. P. Are We Seeing a Resurgence in the Use of Natural Products for New Drug Discovery? *Expert Opin. Drug Discov.* 2019, 14, 417−420.

(30) da Costa, K. S.; Galúcio, J. M.; de Jesus, D. A.; Gomes, G. C.; Lima e Lima, A. H.; Taube, P. S.; dos Santos, A. M.; Lameira, J. Targeting Peptidyl-Prolyl Cis-Trans Isomerase NIMA-Interacting 1: A Structure-Based Virtual Screening Approach to Find Novel Inhibitors. *Curr. Comput.-Aided Drug Des.* 2019, 15, DOI: 10.2174/1573409915666191025114009

(31) Pavela, R. Insecticidal and Repellent Activity of Selected Essential Oils against of the Pollen Beetle, Meligethes Aeneus (Fabricius) Adults. *Ind. Crops Prod.* **2011**, *34*, 888−892.

(32) Nerio, L. S.; Olivero-Verbel, J.; Stashenko, E. E. Repellent Activity of Essential Oils from Seven Aromatic Plants Grown in Colombia against Sitophilus Zeamais Motschulsky (Coleoptera). *J. Stored Prod. Res.* **2009**, *45*, 212−214.

(33) Araújo, E.; Lima, A. H.; Lameira, J. Catalysis by Solvation Rather than the Desolvation Effect: Exploring the Catalytic Efficiency of SAM-Dependent Chlorinase. *Phys. Chem. Chem. Phys.* **2017**, *19*, 21350−21356.

(34) Dos Santos, A. M.; Lima, A. H.; Alves, C. N.; Lameira, J. Unraveling the Addition-Elimination Mechanism of EPSP Synthase through Computer Modeling. *J. Phys. Chem. B* **2017**, *121*, 8626−8637.

(35) da Costa, K. S.; Galúcio, J. M. P.; Leonardo, E. S.; Cardoso, G.; Leal, É.; Conde, G.; Lameira, J. Structural and Evolutionary Analysis of Leishmania Alba Proteins. *Mol. Biochem. Parasitol.* **2017**, *217*, 23−31.

(36) de Alencar, N. A. N.; Sousa, P. R. M.; Silva, J. R. A.; Lameira, J.; Alves, C. N.; Martí, S.; Moliner, V. Computational Analysis of Human OGA Structure in Complex with PUGNAc and NAG-Thiazoline Derivatives. *J. Chem. Inf. Model.* **2012**, *52*, 2775−2783.

(37) Da Costa, K. S.; Leal, E.; Dos Santos, A. M.; Lima E Lima, A. H.; Alves, C. N.; Lameira, J. Structural Analysis of Viral Infectivity Factor of HIV Type 1 and Its Interaction with A3G, EloC and EloB. *PLoS One* **2014**, *9*, No. e89116.

(38) Kumari, S.; Pundhir, S.; Priya, P.; Jeena, G.; Punetha, A.; Chawla, K.; Jafaree, Z. F.; Mondal, S.; Yadav, G. EssOilDB: A Database of Essential Oils Reflecting Terpene Composition and Variability in the Plant Kingdom. *Database* **2014**, *2014*, bau120.

(39) Tsitsanou, K. E.; Thireou, T.; Drakou, C. E.; Koussis, K.; Keramioti, M. V.; Leonidas, D. D.; Eliopoulos, E.; Iatrou, K.; Zographos, S. E. Anopheles Gambiae Odorant Binding Protein Crystal Complex with the Synthetic Repellent DEET: Implications for Structure-Based Design of Novel Mosquito Repellents. *Cell. Mol. Life Sci.* **2012**, *69*, 283−297.

(40) Tabari, M. A.; Youssefi, M. R.; Maggi, F.; Benelli, G. Toxic and Repellent Activity of Selected Monoterpenoids (Thymol, Carvacrol and Linalool) against the Castor Bean Tick, Ixodes Ricinus (Acari: Ixodidae). *Vet. Parasitol.* **2017**, *245*, 86−91.

(41) Youssefi, M. R.; Tabari, M. A.; Esfandiari, A.; Kazemi, S.; Moghadamnia, A. A.; Sut, S.; Dall'Acqua, S.; Benelli, G.; Maggi, F. Efficacy of Two Monoterpenoids, Carvacrol and Thymol, and Their Combinations against Eggs and Larvae of the West Nile Vector Culex Pipiens. *Molecules* **2019**, *24*, 1867.

(42) Pandey, S. K.; Upadhyay, S.; Tripathi, A. K. Insecticidal and Repellent Activities of Thymol from the Essential Oil of Trachyspermum Ammi (Linn) Sprague Seeds against Anopheles Stephensi. *Parasitol. Res.* **2009**, *105*, 507−512.

(43) Mar, J. M.; Silva, L. S.; Azevedo, S. G.; França, L. P.; Goes, A. F. F.; dos Santos, A. L.; de A. Bezerra, J.; Nunomura, R. D. C. S.; Machado, M. B.; Sanches, E. A. Lippia Origanoides Essential Oil: An Efficient Alternative to Control Aedes Aegypti, Tetranychus Urticae and Cerataphis Lataniae. *Ind. Crops Prod.* **2018**, *111*, 292−297.

(44) Elango, G.; Bagavan, A.; Kamaraj, C.; Abduz Zahir, A.; Abdul Rahuman, A. Oviposition-Deterrent, Ovicidal, and Repellent Activities of Indigenous Plant Extracts against Anopheles Subpictus Grassi (Diptera: Culicidae). *Parasitol. Res.* **2009**, *105*, 1567−1576.

(45) Bedini, S.; Flamini, G.; Cosci, F.; Ascrizzi, R.; Echeverria, M. C.; Gomez, E. V.; Guidi, L.; Landi, M.; Lucchi, A.; Conti, B. Toxicity and Oviposition Deterrence of Essential Oils of Clinopodium Nubigenum and Lavandula Angustifolia against the Myiasis-Inducing Blowfly Lucilia Sericata. *PLoS One* **2019**, *14*, No. e0212576.

(46) Pereira, S. I.; Santos, P. A. G.; Barroso, J. G.; Figueiredo, A. C.; Pedro, L. G.; Salgueiro, L. R.; Deans, S. G.; Scheffer, J. J. C. Chemical Polymorphism of the Essential Oils from Populations OfThymus Caespititius Grown on the Islands Pico, Faial and Graciosa (Azores). *Phytochem. Anal.* **2003**, *14*, 228−231.

(47) Rice, P. J.; Coats, J. R. Insecticidal Properties of Monoterpenoid Derivatives to the House Fly (Diptera: Muscidae) and Red Flour Beetle (Coleoptera: Tenebrionidae). *Pestic. Sci.* **1994**, *41*, 195−202.

(48) You, C. X.; Jiang, H. Y.; Zhang, W. J.; Guo, S. S.; Yang, K.; Lei, N.; Ma, P.; Geng, Z. F.; Du, S. S. Contact Toxicity and Repellency of the Main Components from the Essential Oil of Clausena Anisum-Olens against Two Stored Product Insects. *J. Insect Sci.* **2015**, *15*, 87.

(49) Kröber, T.; Koussis, K.; Bourquin, M.; Tsitoura, P.; Konstantopoulou, M.; Awolola, T. S.; Dani, F. R.; Qiao, H.; Pelosi, P.; Iatrou, K.; et al. Odorant-Binding Protein-Based Identification of Natural Spatial Repellents for the African Malaria Mosquito Anopheles Gambiae. *Insect Biochem. Mol. Biol.* **2018**, *96*, 36−50.

(50) Liang, J. Y.; Guo, S. S.; Zhang, W. J.; Geng, Z. F.; Deng, Z. W.; Du, S. S.; Zhang, J. Fumigant and Repellent Activities of Essential Oil Extracted from Artemisia Dubia and Its Main Compounds against Two Stored Product Pests. *Nat. Prod. Res.* **2018**, *32*, 1234−1238.

(51) Wogulis, M.; Morgan, T.; Ishida, Y.; Leal, W. S.; Wilson, D. K. The Crystal Structure of an Odorant Binding Protein from Anopheles Gambiae: Evidence for a Common Ligand Release Mechanism. *Biochem. Biophys. Res. Commun.* **2006**, *339*, 157−164.

(52) Tzotzos, G.; Iley, J. N.; Moore, E. A. New Insights on Repellent Recognition by Anopheles Gambiae Odorant-Binding Protein 1. *PLoS One* **2018**, *13*, No. e0194724.

(53) Manoharan, M.; Fuchs, P. F. J.; Sowdhamini, R.; Offmann, B. Insights on PH-Dependent Conformational Changes of Mosquito Odorant Binding Proteins by Molecular Dynamics Simulations. *J. Biomol. Struct. Dyn.* **2014**, *32*, 1742−1751.

(54) Yu, H.; Zhao, X.; Feng, X. L.; Chen, X.; Borowiak-Palen, E.; Huang, X. R. Molecular Simulations Study of Ligand-Release Mechanism in an Odorant-Binding Protein from the Southern House Mosquito. *J. Biomol. Struct. Dyn.* **2013**, *31*, 485−494.

(55) Naïm, M.; Bhat, S.; Rankin, K. N.; Dennis, S.; Chowdhury, S. F.; Siddiqi, I.; Drabik, P.; Sulea, T.; Bayly, C. I.; Jakalian, A.; et al. Solvated Interaction Energy (SIE) for Scoring Protein-Ligand Binding Affinities. 1. Exploring the Parameter Space. *J. Chem. Inf. Model.* **2007**, *47*, 122−133.

(56) Anselmi, C.; Buonocore, A.; Centini, M.; Facino, R. M.; Hatt, H. The Human Olfactory Receptor 17-40: Requisites for Fitting into the Binding Pocket. *Comput. Biol. Chem.* **2011**, *35*, 159−168.

(57) Santana, I. B.; Leite, F. H. A.; Santos Junior, M. C. Identification of Lutzomyia Longipalpis Odorant Binding Protein Modulators by Comparative Modeling, Hierarchical Virtual Screening, and Molecular Dynamics. *J. Chem.* **2018**, *2018*, 1−10.

(58) ChemAxon Ltd. *Marvin.* http://www.chemaxon.com: Budapest 2014.

(59) Bajusz, D.; Rácz, A.; Héberger, K. Why Is Tanimoto Index an Appropriate Choice for Fingerprint-Based Similarity Calculations? *J. Cheminform.* **2015**, *7*, 20.

(60) Sunseri, J.; Koes, D. R. Pharmit: Interactive Exploration of Chemical Space. *Nucleic Acids Res.* **2016**, *44*, W442−W448.

(61) Thomsen, R.; Christensen, M. H. MolDock: A New Technique for High-Accuracy Molecular Docking. *J. Med. Chem.* **2006**, *49*, 3315−3321.

(62) De Azevedo, W., Jr. MolDock Applied to Structure-Based Virtual Screening. *Curr. Drug Targets* **2010**, *11*, 327−334.

(63) Case, D. A.; Cheatham, T. E.; Darden, T.; Gohlke, H.; Luo, R.; Merz, K. M.; Onufriev, A.; Simmerling, C.; Wang, B.; Woods, R. J. The Amber Biomolecular Simulation Programs. *J. Comput. Chem.* **2005**, *26*, 1668−1688.

(64) Wang, J.; Cieplak, P.; Kollman, P. A. How Well Does a Restrained Electrostatic Potential (RESP) Model Perform in Calculating Conformational Energies of Organic and Biological Molecules? *J. Comput. Chem.* **2000**, *21*, 1049−1074.

(65) Frisch, M. J.et al. *Gaussian 09. Gaussian, Inc. Wallingford CT.* Gaussian Inc.: Wallingford CT 2009, pp 2−3.

(66) Echenique, P.; Alonso, J. L. A Mathematical and Computational Review of Hartree-Fock SCF Methods in Quantum Chemistry. *Mol. Phys.* **2007**, *105*, 3057−3098.

(67) Ditchfield, R.; Hehre, W. J.; Pople, J. A. Self-Consistent Molecular-Orbital Methods. IX. An Extended Gaussian-Type Basis for Molecular-Orbital Studies of Organic Molecules. *J. Chem. Phys.* **1971**, *54*, 724−728.

(68) Mark, P.; Nilsson, L. Structure and Dynamics of the TIP3P, SPC, and SPC/E Water Models at 298 K. *J. Phys. Chem. A* **2001**, *105*, 9954−9960.

(69) Maier, J. A.; Martinez, C.; Kasavajhala, K.; Wickstrom, L.; Hauser, K. E.; Simmerling, C. Ff14SB: Improving the Accuracy of Protein Side Chain and Backbone Parameters from Ff99SB. *J. Chem. Theory Comput.* **2015**, *11*, 3696−3713.

(70) Wang, J.; Wolf, R. M.; Caldwell, J. W.; Kollman, P. A.; Case, D. A. Development and Testing of a General Amber Force Field. *J. Comput. Chem.* **2004**, *25*, 1157−1174.

(71) Kräutler, V.; Van Gunsteren, W. F.; Hünenberger, P. H. A Fast SHAKE Algorithm to Solve Distance Constraint Equations for Small Molecules in Molecular Dynamics Simulations. *J. Comput. Chem.* **2001**, *22*, 501−508.

(72) Scheurer, M.; Rodenkirch, P.; Siggel, M.; Bernardi, R. C.; Schulten, K.; Tajkhorshid, E.; Rudack, T. PyContact: Rapid, Customizable, and Visual Analysis of Noncovalent Interactions in MD Simulations. *Biophys. J.* **2018**, *114*, 577−583.

(73) Humphrey, W.; Dalke, A.; Schulten, K. VMD: Visual Molecular Dynamics. *J. Mol. Graph.* **1996**, *14*, 33−38 27−28.

(74) Sittel, F.; Jain, A.; Stock, G. Principal Component Analysis of Molecular Dynamics: On the Use of Cartesian vs. Internal Coordinates. *J. Chem. Phys.* **2014**, *141*, No. 014111.

(75) Kumari, P.; Poddar, R. A Comparative Multivariate Analysis of Nitrilase Enzymes: An Ensemble Based Computational Approach. *Comput. Biol. Chem.* **2019**, *83*, 107095.

(76) Neves Cruz, J.; Santana de Oliveira, M.; Gomes Silva, S.; Pedro da Silva Souza Filho, A.; Santiago Pereira, D.; Lima e Lima, A. H.; de Aguiar Andrade, E. H. Insight into the Interaction Mechanism of Nicotine, NNK, and NNN with Cytochrome P450 2A13 Based on Molecular Dynamics Simulation. *J. Chem. Inf. Model.* **2019**, acs.jcim.9b00741.

(77) Costa, C. H. S.; Oliveira, A. R. S.; dos Santos, A. M.; da Costa, K. S.; Lima, A. H. L. E.; Alves, C. N.; Lameira, J. Computational Study of Conformational Changes in Human 3-Hydroxy-3-Methylglutaryl Coenzyme Reductase Induced by Substrate Binding. *J. Biomol. Struct. Dyn.* **2019**, 4374−4383.

(78) Chen, J. Functional Roles of Magnesium Binding to Extracellular Signal-Regulated Kinase 2 Explored by Molecular Dynamics Simulations and Principal Component Analysis. *J. Biomol. Struct. Dyn.* **2018**, *36*, 351−361.

(79) Maisuradze, G. G.; Leitner, D. M. Free Energy Landscape of a Biomolecule in Dihedral Principal Component Space: Sampling Convergence and Correspondence between Structures and Minima. *Proteins* **2007**, *67*, 569−578.

(80) Roe, D. R.; Cheatham, T. E., III PTRAJ and CPPTRAJ: Software for Processing and Analysis of Molecular Dynamics Trajectory Data. *J. Chem. Theory Comput.* **2013**, *9*, 3084−3095.

(81) Grant, B. J.; Rodrigues, A. P. C.; ElSawy, K. M.; McCammon, J. A.; Caves, L. S. D. Bio3d: An R Package for the Comparative Analysis of Protein Structures. *Bioinformatics* **2006**, *22*, 2695−2696.

(82) Cui, Q.; Sulea, T.; Schrag, J. D.; Munger, C.; Hung, M. N.; Naïm, M.; Cygler, M.; Purisima, E. O. Molecular Dynamics-Solvated Interaction Energy Studies of Protein-Protein Interactions: The MP1-P14 Scaffolding Complex. *J. Mol. Biol.* **2008**, *379*, 787−802.

(83) Genheden, S.; Ryde, U. The MM/PBSA and MM/GBSA Methods to Estimate Ligand-Binding Affinities. *Expert Opin. Drug Discov.* **2015**, *10*, 449−461.

(84) Avram, S.; Funar-Timofei, S.; Borota, A.; Chennamaneni, S. R.; Manchala, A. K.; Muresan, S. Quantitative Estimation of Pesticide-Likeness for Agrochemical Discovery. *J. Cheminform.* **2014**, *6*, 42.